Research Article Vol. 31, No. 4 / 13 Feb 2023 / Optics Express 5378
Optics EXPRESS

Electrically tuned active metasurface towards metasurface-integrated liquid crystal on silicon (meta-LCoS) devices

XIN CHANG, MIKE PIVNENKO, PAWAN SHRESTHA, WEIJIE WU, WENHAN ZHANG, AND DAPING CHU*

Centre for Photonic Devices and Sensors, University of Cambridge, 9 JJ Thompson Avenue, Cambridge CB3 0FA, United Kingdom
dpc31@cam.ac.uk

Abstract: Active metasurfaces add a new dimension to static metasurfaces by introducing tunability, and this has received enormous attention from industry. Although various mechanisms have been proposed over the past few years in literature, solutions with good practicality are limited. Liquid crystal (LC)-based active metasurface is one of the most promising approaches due to the well-established LC industry. In this paper, an electrically tunable active metasurface was proposed and experimentally demonstrated using photoaligned nematic LC. The good quality of the LC photoalignment on the metasurface was demonstrated. Tunable transmission was obtained for telecommunication C band and the modulation depth in transmission amplitude of 94% was realized for 1530 nm. Sub-millisecond response time was achieved at operating a temperature of 60°C. The progress made here presents the potential of LC-based active metasurfaces for fast-switching photonic devices at optical communication wavelengths. More importantly, this work lays the foundations for the next-generation liquid crystal on silicon (LCoS) devices that are integrated with metasurfaces (meta-LCoS).

Published by Optica Publishing Group under the terms of the Creative Commons Attribution 4.0 License. Further distribution of this work must maintain attribution to the author(s) and the published article's title, journal citation, and DOI.

1. Introduction

Metasurface has become a powerful tool to tailor the light-matter interaction at the sub-wavelength scale. As the two-dimensional counterpart of metamaterial, metasurface is typically composed of subwavelength nanostructures that are distributed in a planar lattice with subwavelength lattice constant. Over the past decade, it has been extensively reported in a variety of applications such as computer-generated holography [1,2], imaging optics [3,4], spatial light modulators [5,6] etc., because of its unique access to light properties like phase, amplitude, polarization, angular momentum [7,8] etc. Recently, the functionalities of metasurface were further expanded by active metasurface [9–11], which provides tunability for conventional static metasurface. The tunability has been realized through several mechanisms, including tunable dielectric environment of metasurface using liquid crystal (LC) [12–18], tunable refractive index of metasurface itself using phase-changing material (PCM) [19,20], semiconducting material through charge carrier density modulation [20–22], conducting polymers through electrochemical process [23] etc. However, only a limited number of solutions can outcompete or be compatible with currently existing devices, especially those used in the visible and near infrared wavelengths. LC-based active metasurface is one of the most promising approaches because LC technology has become highly advanced after decades of development in LC-based devices such as LC displays (LCDs) and LC on silicon (LCoS) spatial light modulators (SLMs). Not only does LC material provide electrically controllable refractive index, but it is also scalable and economic. This makes LC-based active metasurface highly promising for practical applications.

#483452 https://doi.org/10.1364/OE.483452
Journal © 2023 Received 13 Dec 2022; revised 11 Jan 2023; accepted 20 Jan 2023; published 30 Jan 2023

Optics EXPRESS

LC is an anisotropic optical material with uniaxial symmetry of the dielectric permittivity. Due to the strong dipole moment, LC molecule orientation follows the direction of electric field vector and can be rotated with low driving voltage. As a result, linearly polarized light with polarization direction along the LC director experiences a variable index of refraction if the applied voltage is changed. Although numerous efforts have been made by researchers to develop LC-based active metasurface (hereafter referred to as LCAM), it is still challenging. Early attempt to tune the metasurface resonance wavelength by temperature was reported [14] The spectral position of the electric dipole mode and magnetic dipole mode were simultaneously tuned by raising temperature from 21 to 62°C. Electric dipole resonance experienced a larger spectral shift of 40 nm around 1650 nm compared to the magnetic one. Similarly, other researchers reported spectral tuning of Fano resonance with high quality factor from 1010 nm to around 1000 nm with nematic LC by raising temperature up to 80°C [24]. Temperature-controlled LCAM has limited response speed and spatial resolution, and hence electrical tuning of LCAM has been investigated lately. A spectral shift of about 50 nm and 25 nm, for magnetic dipole mode and electric dipole mode respectively, was experimentally recorded at optical communication wavelengths with a voltage range from 0 to 70 V [13]. The required high driving voltage poses a huge challenge for practical applications. A wider redshift of 110 nm was achieved with gap plasmon resonance for a zigzag plasmonic metasurface with the voltage variation of 2.7 V [16]. Plasmonic metasurface, however, is not ideal for modulating light with high frequency due to the dominant Ohmic loss and the accompanying low efficiency. So far, electrical tuning of LCAM made from dielectric material has not been realized for optical communication C band (1530-1565 nm) with relatively small voltage variation. Moreover, this work demonstrates the potential for metasurface-integrated liquid crystal on silicon (LCoS) devices (meta-LCoS) [25–34].

In this paper, a dielectric LCAM with a tunable resonance in range of 1524-1573 nm was realized via voltage variation between 0 V and 10 V. The design and simulation of LCAM are presented in section 2. The characterization of LC alignment in an LCAM cell is discussed in section 3. Finally, the resonance tuning is experimentally demonstrated in section 4 with sub-millisecond switching time. The large amplitude modulation and fast switching of the demonstrated LCAM device provides a highly practical option for optical switches in telecommunication networks. It also enables a wide range of optical functionalities that are based on amplitude modulation, such as diffractive optics [35,36] and holograms [37,38].

2. LCAM design and simulation

The metasurface was fabricated from amorphous silicon because it has high index of refraction $n \sim 3.48$ and negligible loss at the target center wavelength is 1550 nm. The metasurface consists of an array of nanodisks that are periodically distributed in a square lattice. The structure of the LCAM unit cell is illustrated on the left of Fig. 1(a). The silicon nanodisks are sitting on top of ITO-coated borosilicate glass substrate (n ~ 1.50 at 1550 nm) and another ITO-coated borosilicate glass is used as the ceiling of LCAM cell. ITO is index-matched with glass. Both substrates are further coated with azobenzene (AZB) for LC photoalignment (the alignment direction is in X direction). ITO layer and AZB layer are represented in blue and yellow in Fig. 1(a), respectively. The cell gap is maintained at 1μm by glass spacers mixed with the encapsulation glue. The cell is filled with nematic LC. The extraordinary index $n_e = 1.68$ and ordinary index $n_o = 1.50$ were used in the simulation at 1550 nm. The index values are based on the data provided by the supplier and our own measurements. LC absorption is neglected at this wavelength. For the simulation the LC is assumed to be homogeneously aligned with the LC director in X direction with no voltage applied. Anisotropic dielectric properties of the LC can be expressed by its dielectric permittivity tensor $R[\varepsilon]R^{\dagger}$, where $[\varepsilon]$ is the standard permittivity tensor of uniaxial crystal in its diagonal form and R is the unitary rotation matrix. † denotes the complex conjugate. In this case, only the LC rotation in XY plane (quantified by angle θ between LC director and X axis) is

Optics EXPRESS

considered so the rotation matrix $R[\varepsilon]R^{\dagger}$ is simplified to be a function of angle θ in a 3×3 matrix. The LCAM sample is illuminated at normal incidence from the top with linearly polarized light with polarization in X direction

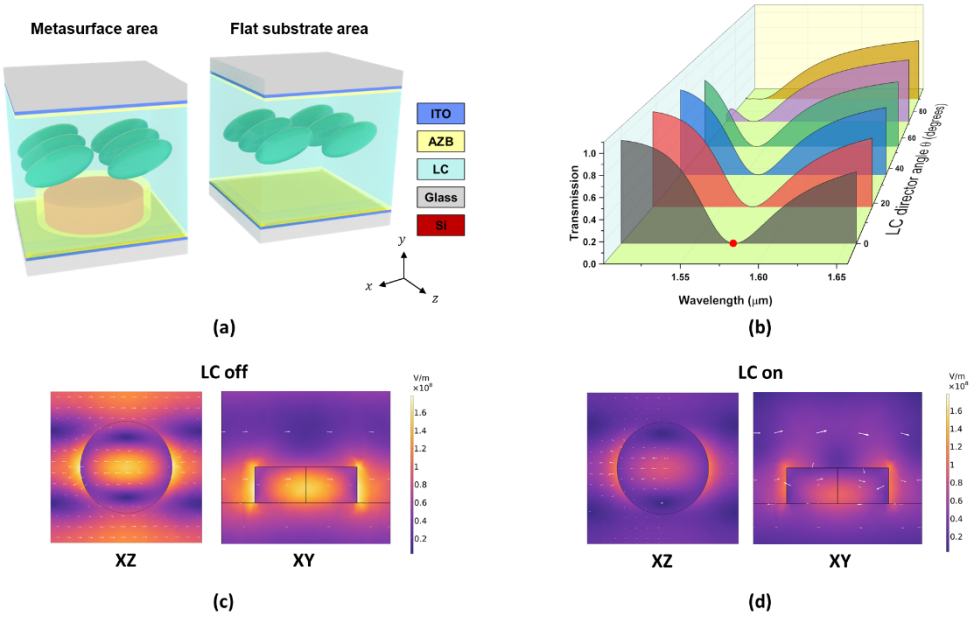

Fig. 1. (a) The structure of LCAM unit cell. LCAM cell is illuminated with linearly polarized light (along Z direction) at normal incidence. (b) Simulated transmission spectrum of the LCAM at various LC director angles θ from 0° to 90°. The electric field distribution at 1575 nm in XY plane and XZ plane when LC is off (c) and on (d).

Nanodisk dimensions (height h, diameter d) and lattice constant p are selected so that the resonance is located at the desired spectral position. In this case, height $h = 190$ nm, diameter $d = 560$ nm and lattice constant $p = 890$ nm were chosen to get the resonance at about 1575 nm. The full-wave simulation for the LC orientation in a range of θ from 0° to 90°, which translates to the indices of refraction experienced by the incident polarized light from 1.68 to 1.50, was carried out. The simulated transmission spectrum is shown in Fig. 1(b). When θ is 0° (black curve), the transmission reaches a minimum at 1575 nm (denoted by a red dot). Its electric field distribution was further illustrated in Fig. 1(c), which shows the dominant electric dipole resonance. The simulated transmission spectrum for larger θ (smaller index of refraction) was also plotted in Fig. 1(b), which indicates that a smaller effective refractive index induces a blue shift of the resonance. The electric field for $\theta = 90°$ at 1575 nm was plotted in Fig. 1(d), which showed a weakened resonance. Therefore, the resonance strength was tuned by LC rotation.

3. LCAM cell fabrication and LC alignment

An LCAM cell was fabricated to investigate the alignment quality of LC and tunability of the resonance. The process flow is shown in Fig. 2(a). Silicon metasurface was created by firstly sputtering 190 nm thick amorphous silicon thin film on ITO-coated borosilicate glass. Then PMMA photoresist (Kayaku Advanced Materials) was spin-coated on top, followed by standard electron beam lithography process. The structure was transferred to silicon through liftoff and fluorine-based reactive ion etching. The SEM image and optical image of the fabricated nanodisk metasurface are also depicted in Fig. 2(a). The overall area of the metasurface is 0.8 mm × 0.8 mm.

Optics EXPRESS

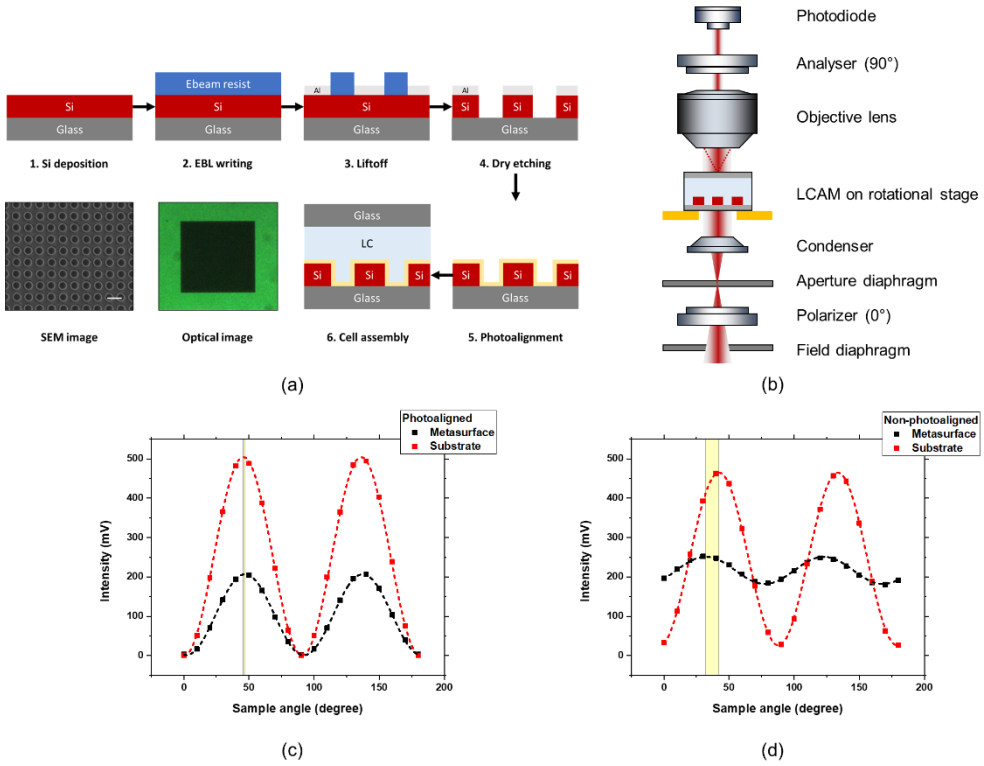

Fig. 2. (a) Process flow of LCAM device fabrication. The inset images are SEM image and optical image of the fabricated device. Scale bar: 1 µm. (b) The setup for transmission measurement. Sample was illuminated from the bottom. (c) The measured output light intensity against in-plane LC director angle (φ) for the metasurface area (black) and the reference area (red). (d) Same measurement was conducted for another sample without photoalignment on metasurface substrate.

LC alignment is critical to electrically controlled birefringence (ECB) configuration used in this paper. Due to the presence of the non-flat metasurface on one of the substrates, the usual LC alignment by rubbing was not practical. Instead, we used photoalignment to align the LC.

A layer of AZB was firstly spin-coated from prepared AZB solution, which was a mixture of Poly[1-[4-(3-carboxy-4-hydroxyphenylazo)benzenesulfonamido]-1,2-ethanediyl, sodium salt] (Sigma-Aldrich) and deionized water with a weight ratio of 1:1000. AZB was also spin-coated on the top substrate. After dispensing the glue and spacers mixture near the boundary of substrate, two substrates were placed in tight contact with each other. The glue was then cured with UV light and the cell was illuminated with linearly polarized light (405 nm, 10 mW, 3 minutes) for photoalignment. Finally, the LCAM cell was filled with nematic LC (MDA-98-1602, Merck) at the temperature of 115°C.

The quality of the LC alignment was quantitatively characterized by measuring the light transmittance of the cell placed between a pair of crossed polarizers in a microscope setup, as it is shown in Fig. 2(b). The measurement was conducted using a visible light with wavelength of 543 nm. The LCAM sample was fixed onto a rotational stage so that the azimuth angle (φ) in XZ plane of the LCAM cell can be adjusted. The field diaphragm and the aperture diaphragm were used to restrict the light passing through the system to an area within the metasurface and to a cone angle of ±3°. This is to ensure illumination with nearly collimated light. The intensity of

Optics EXPRESS

the transmitted light (I_{out}) was measured with a photodetector (PDA36A2, Thorlabs) at various angles φ of the LCAM cell.

The results in Fig. 2(c) show experimentally measured the intensity of the transmitted light for the metasurface area (black squares) and for the neighboring flat substrate area (red squares) of the same cell as a reference. The LC in the metasurface area is aligned by AZB coated on the flat top substrate and the metasurface substrate. Reference measurement was conducted for the LC aligned by AZB coated on both flat substrates.

According to the Jones matrix of uniaxial crystal, the light intensity after analyzer I_{out} is related to the φ angle of LC director by $I_{out} \propto \sin^2(\varphi)$. The dashed lines in Figs. 2(c) and (d) are the fitted curves. The quality of LC alignment can be quantified by the contrast ratio $CR = I_{max}/I_{min}$, where I_{max} and I_{min} are the maximum and minimum intensity of the transmitted light. For the reference flat substrate area, I_{min} was 1.7 mV and the CR was around 300. This sets the benchmark for LC alignment quality. For the metasurface area, $I_{min} = 2.9$ mV and $CR = 71$. The higher I_{min} of the metasurface area results from the distorted LC alignment by the metasurface. The lower CR is also caused by silicon absorption at the visible wavelength. Moreover, the phase shift ($\Delta\varphi$), which is defined as the shift in angle φ between the curves fitted for metasurface area and flat substrate area, is also a good indicator to evaluate the LC alignment quality of the photoaligned metasurface. After curve fitting, the $\Delta\varphi$ was extracted to be 1.6°, as is represented by the narrow yellow area in Fig. 2(d). This proves that the LC alignment of the metasurface area is close to that of the reference area, which signifies a good LC alignment quality by photoaligned metasurface. The measured and extracted parameters are listed in Table 1 below.

Table 1. Measured and extracted parameters for photoaligned and non-photoaligned samples

Parameters		I_{max} (measurement)	I_{min} (measurement)	CR (measurement)	ΔI (curve fitting)	$\Delta\varphi$ (curve fitting)
Unit		mV	mV		mV	degree
Photoaligned	Metasurface	206.7	2.9	71	206	1.6
	Substrate	504.5	1.7	300	504	
Non - Photoaligned	Metasurface	251.1	180	1.4	69	9.8
	Substrate	465.1	28.9	16	439	

In order to demonstrate the effect of the metasurface on the LC alignment experimentally, a different LCAM cell was fabricated. In this case, AZB was spin-coated on metasurface, but it was not photoaligned. The top substrate without metasurface was photoaligned as usual. The same measurement was completed for the metasurface area and the flat substrate area, Fig. 2(d). The $I_{min} = 180$ mV, $CR = 1.4$ for the metasurface area and $I_{min} = 28.9$ mV, $CR = 16$ for the flat substrate area and the phase shift $\Delta\varphi$ was 9.8°. These parameters are also listed in Table 1. The increased I_{min} level, smaller CR and larger phase shift of $\Delta\varphi$ all denote a stronger disruption on LC alignment by non-photoaligned metasurface compared to photoaligned metasurface shown in Fig. 2(c).

To conclude this section, the LC alignment in the photoaligned metasurface prepared following our procedure shows a good uniformity which is highly important for LCAM devices. Future research on theoretical calculation of LC's interaction with nanostructures using minimal free energy [15,39] could be very helpful to fully understand and better utilize this type of devices.

4. Electrical tuning of metasurface resonance wavelength

The metasurface resonance tuning was realized by altering the effective refractive index of LC surrounding the metasurface, which is implemented through an external voltage. A square-wave

Optics EXPRESS

AC voltage of 2 kHz was applied to the LCAM cell with the peak amplitude V_p in a range from 0 to 10 V. The cell was illuminated by linearly polarized light with polarization direction parallel to the LC director. An analyzer was also aligned in the same direction (polarizer: 0°, analyzer: 0°). The transmission spectrum was measured with a spectrometer (NIRQuest, Ocean Optics). The results are shown in Fig. 3(a). A transmission minimum due to the metasurface resonance was observed within the telecommunication C band wavelength. The spectral position of the transmission minimum shifts from 1573 to 1524 nm as V_p increases from 0 to 10 V, indicated by white dashed lines in Fig. 3(a). This provides a working bandwidth of around 50 nm, which covers the optical communication C band (1530-1565 nm). The transmission at 1530 nm was tuned from 83.5% ($V_p = 0$ V, off state) to 9.5% ($V_p = 10$ V, on state), which corresponds to a transmission variation (T_{off}/T_{on}) of about 8.8 times and a modulation depth ($\Delta T/T_{off}$) of 89%. This is equivalent to a modulation depth in transmission amplitude of 94%. The tunability can be further improved by using LC with a larger birefringence, which provides a larger variation in refractive index of the dielectric environment for metasurface.

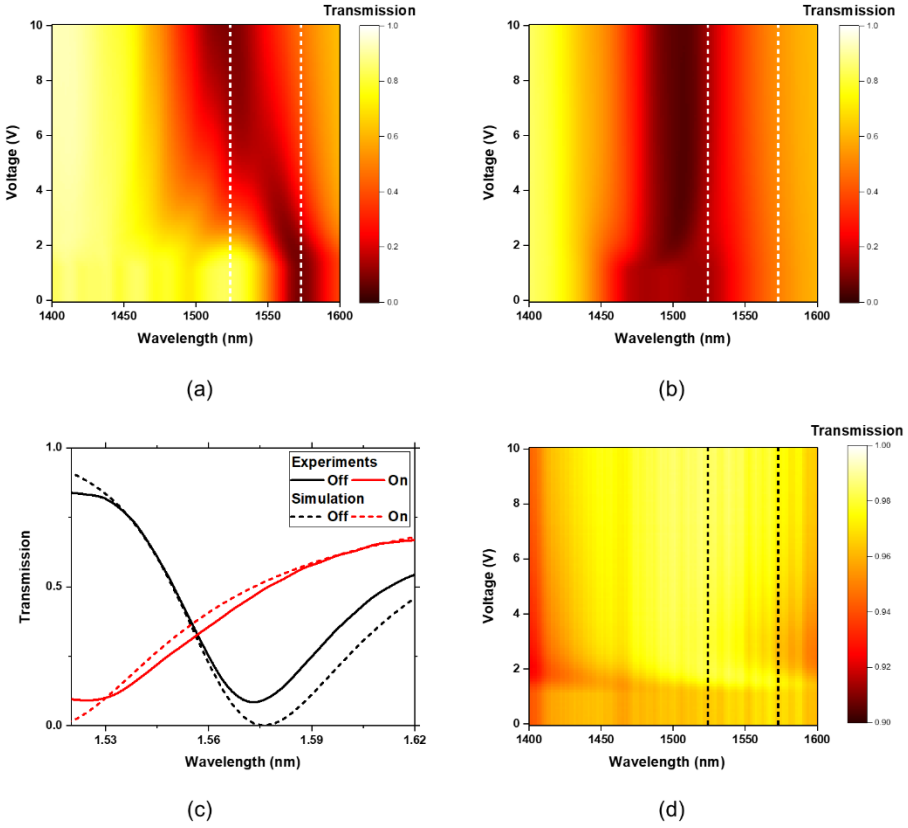

Fig. 3. The measured co-polarized component of the transmitted light for incident polarizations (a) parallel and (b) orthogonal to the LC director. (c) The comparison between simulated transmission (dashed lines) and measured transmission (solid lines) when the LCAM cell is in the on (red) and off (black) states. (d) The same measurement as (a) was performed for a pure LC cell.

The same measurement was conducted for incident light polarized orthogonally to the LC director (polarizer: 90°, analyzer: 90°). The results are shown in Fig. 3(b). It clearly shows that there is no obvious change in transmission for the wavelength of interest. This is because the

Optics EXPRESS

effective refractive index (ordinary index of refraction) is not affected by the increasing voltages. The experimentally measured transmission spectrum is compared with that from the simulation in section 2. The comparison for $V_p = 10$ V is shown in Fig. 3(c). The spectral position of transmission minimum obtained from measurement is consistent with that from simulation. The measured transmission minimum (<10%) is higher than the simulated value. This is partly due to the negligence of absorption by silicon at 1550 nm in the simulation model and partly due to some fabrication imperfections.

As a comparison, the same measurement was performed for a reference area of the LC cell without metasurface (polarizer: 0°, analyzer: 0°). No transmission minimum was observed, as is shown in Fig. 3(d). The transmission colormap has a range of 0.9 ~ 1. At least 90% transmission was recorded over the wavelength of interest. The small variation in transmission under different voltages comes from the cavity interference effect of the LC cell.

Switching speed is critical to active devices and sub-millisecond switching is always desired in industrial applications. This has been a challenge for LC-based devices operating at optical telecommunication wavelength. The response time (τ) of LCAM was measured with a tunable laser (T100S-HP, EXFO) and a photodiode (PDA20CS2, Thorlabs) across the C band and temperature range 30-70°C. The driving voltage with $V_P = 10$ V and the frequency of 2 kHz was used. The switching time of the LCAM device operated under 1525 nm wavelength was determined by extracting the time of the normalized transmission with 20/80% variation. The

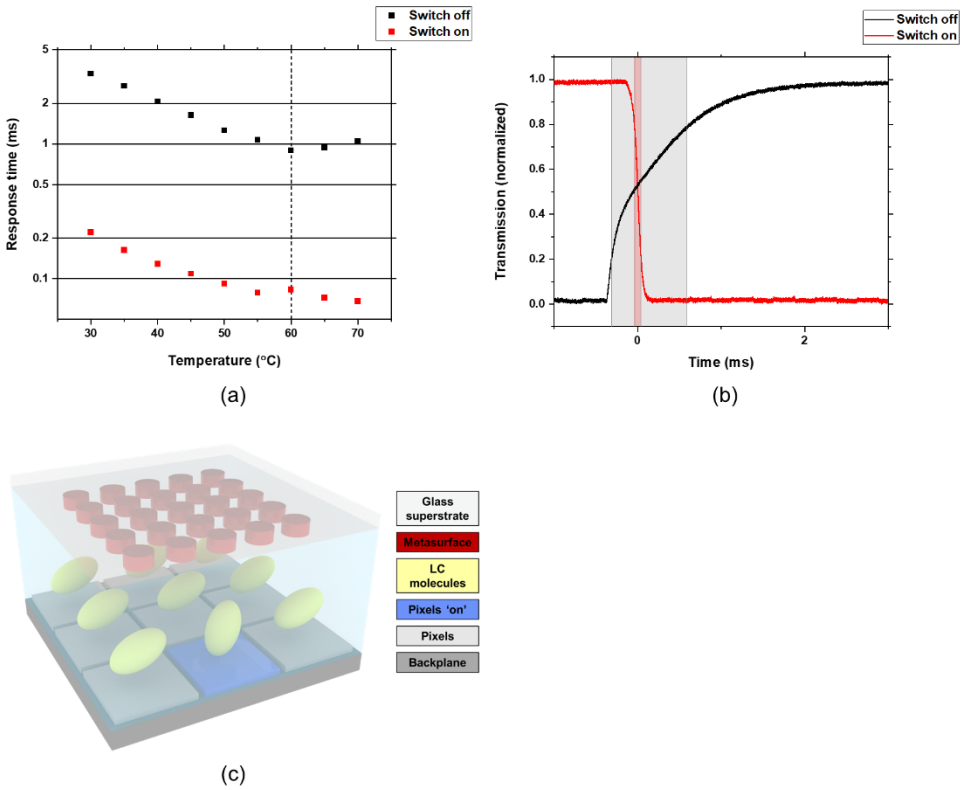

Fig. 4. (a) The temperature dependence of the switching on and switching off time of the LCAM device operated at 1520 nm. (b) The switching on and off characteristics of the LCAM device for 1525 nm at 60°C. (c) An illustration of metasurface-integrated LCoS devices.

Optics EXPRESS

time for switching on (τ_{on}) and switching off (τ_{off}) were measured to be 0.22 ms / 3.32 ms, respectively at 30°C. The switching off process is slower than the switching on process because the former is dominated by the anchoring force and intermolecular Van der Waals force, which are relatively weaker than the electric force under high driving voltage. The temperature dependence of the response time is shown in Fig. 4(a). Both τ_{on} and τ_{off} decrease at higher temperature as a result of viscosity reduction with $\tau_{on} = 0.08$ ms and $\tau_{off} = 0.90$ ms for 60°C, which is highly encouraging for practical applications. In terms of the modulation frequency, the maximum achievable modulation frequency is around 1.11 kHz. This is illustrated in Fig. 4(b), in which the transient measurement of the switching on and switching off process was demonstrated.

The sub-millisecond switching speed is highly attractive for LC-based devices operated in near infrared wavelengths. The ultrathin nature of metasurface can relieve the thickness constraint of the conventional LCoS devices and boost the response speed of metasurface-integrated LCoS devices (meta-LCoS), as is schematically shown in Fig. 4(c). The inter-pixel voltage crosstalk can also be effectively reduced with thinner LC cells. This work demonstrated the amplitude modulation feature and future research can be carried out to modulate other dimensions of light such as phase and polarization.

5. Conclusions

An electrically tunable metasurface with a thin layer of photoaligned LC was demonstrated in optical communication C band. Results from both simulation and experiment agreed with each other, showing a blue shift of the resonance with the increase of the control voltage. A resonance shift of 49 nm through the C band was obtained with the applied voltage changed between 0 and 10 V. A maximum modulation depth of 94% in transmission amplitude was recorded at 1530 nm. The high quality of uniform LC alignment was quantitatively evaluated with crossed polarizers. The sub-millisecond switching time of the LCAM was demonstrated at 1525 nm for operating temperature around 60°C. The fast switching speed with sub-millisecond response as demonstrated by the LCAM device is highly valuable for telecommunication applications since LC-based devices operated at telecommunication wavelength typically have a large LC thickness (much more than the 1 μm thick LC used here) and hence relatively slow switching speed. Considering maturity of LC technologies and scalability of silicon nanostructures, the proposed and demonstrated LCAM shows great prospects of active metasurfaces in practical applications.

Funding. Engineering and Physical Sciences Research Council (EP/S022139/1).

Disclosures. The authors declare no conflicts of interest.

Data availability. Data underlying the results presented in this paper are not publicly available at this time but may be obtained from the authors upon reasonable request.

References

1. W. Wan, J. Gao, and X. Yang, "Metasurface Holograms for Holographic Imaging," Adv. Opt. Mater. **5**(21), 1700541 (2017).
2. L. Huang, S. Zhang, and T. Zentgraf, "Metasurface holography: from fundamentals to applications," Nanophotonics **7**(6), 1169–1190 (2018).
3. W. T. Chen, A. Y. Zhu, and F. Capasso, "Flat optics with dispersion-engineered metasurfaces," Nat. Rev. Mater. **5**(8), 604–620 (2020).
4. W. T. Chen, A. Y. Zhu, V. Sanjeev, M. Khorasaninejad, Z. Shi, E. Lee, and F. Capasso, "A broadband achromatic metalens for focusing and imaging in the visible," Nat. Nanotechnol. **13**(3), 220–226 (2018).
5. S.-Q. Li, X. Xu, R. Maruthiyodan Veetil, V. Valuckas, R. Paniagua-Domínguez, and A. I. Kuznetsov, "Phase-only transmissive spatial light modulator based on tunable dielectric metasurface," Science **364**(6445), 1087–1090 (2019).
6. X. Chang, M. Pivnenko, P. Shrestha, W. Wu, and D. Chu, "Increasing Diffraction Angle of LCoS Device through Integration with Metasurface," in *Digital Holography and 3-D Imaging 2022* (Optica Publishing Group, 2022), paper M3A.3.
7. A. I. Kuznetsov, A. E. Miroshnichenko, M. L. Brongersma, Y. S. Kivshar, and B. Luk'yanchuk, "Optically resonant dielectric nanostructures," Science **354**(6314), aag2472 (2016).

Optics EXPRESS

8. A. Arbabi, Y. Horie, M. Bagheri, and A. Faraon, "Dielectric metasurfaces for complete control of phase and polarization with subwavelength spatial resolution and high transmission," Nat. Nanotechnol. **10**(11), 937–943 (2015).
9. A. M. Shaltout, V. M. Shalaev, and M. L. Brongersma, "Spatiotemporal light control with active metasurfaces," Science **364**(6441), eaat3100 (2019).
10. T. Badloe, J. Lee, J. Seong, and J. Rho, "Tunable Metasurfaces: The Path to Fully Active Nanophotonics," Adv Photonics Res **2**(9), 2000205 (2021).
11. Q. He, S. Sun, and L. Zhou, "Tunable/Reconfigurable Metasurfaces: Physics and Applications," Research (Washington, DC, U. S.) **2019**, 1849272 (2019).
12. A. Komar, R. Paniagua-Domínguez, A. Miroshnichenko, Y. F. Yu, Y. S. Kivshar, A. I. Kuznetsov, and D. Neshev, "Dynamic Beam Switching by Liquid Crystal Tunable Dielectric Metasurfaces," ACS Photonics **5**(5), 1742–1748 (2018).
13. A. Komar, Z. Fang, J. Bohn, J. Sautter, M. Decker, A. Miroshnichenko, T. Pertsch, I. Brener, Y. S. Kivshar, I. Staude, and D. N. Neshev, "Electrically tunable all-dielectric optical metasurfaces based on liquid crystals," Appl. Phys. Lett. **110**(7), 071109 (2017).
14. J. Sautter, I. Staude, M. Decker, E. Rusak, D. N. Neshev, I. Brener, and Y. S. Kivshar, "Active Tuning of All-Dielectric Metasurfaces," ACS Nano **9**(4), 4308–4315 (2015).
15. J. A. Dolan, H. Cai, L. Delalande, X. Li, A. B. F. Martinson, J. J. de Pablo, D. López, and P. F. Nealey, "Broadband Liquid Crystal Tunable Metasurfaces in the Visible: Liquid Crystal Inhomogeneities Across the Metasurface Parameter Space," ACS Photonics **8**(2), 567–575 (2021).
16. O. Buchnev, N. Podoliak, M. Kaczmarek, N. I. Zheludev, and V. A. Fedotov, "Electrically Controlled Nanostructured Metasurface Loaded with Liquid Crystal: Toward Multifunctional Photonic Switch," Adv Opt Mater **3**(5), 674–679 (2015).
17. M. Sun, X. Xu, X. W. Sun, X. Liang, V. Valuckas, Y. Zheng, R. Paniagua-Domínguez, and A. I. Kuznetsov, "Efficient visible light modulation based on electrically tunable all dielectric metasurfaces embedded in thin-layer nematic liquid crystals," Sci. Rep. **9**(1), 8673 (2019).
18. Z. Shen, S. Zhou, X. Li, S. Ge, P. Chen, W. Hu, and Y. Lu, "Liquid crystal integrated metalens with tunable chromatic aberration," Adv. Photonics **2**(03), 1 (2020).
19. Y. Wang, P. Landreman, D. Schoen, K. Okabe, A. Marshall, U. Celano, H.-S. P. Wong, J. Park, and M. L. Brongersma, "Electrical tuning of phase-change antennas and metasurfaces," Nat. Nanotechnol. **16**(6), 667–672 (2021).
20. M. C. Sherrott, P. W. C. Hon, K. T. Fountaine, J. C. Garcia, S. M. Ponti, V. W. Brar, L. A. Sweatlock, and H. A. Atwater, "Experimental Demonstration of >230° Phase Modulation in Gate-Tunable Graphene–Gold Reconfigurable Mid-Infrared Metasurfaces," Nano Lett. **17**(5), 3027–3034 (2017).
21. Y.-W. Huang, H. W. H. Lee, R. Sokhoyan, R. A. Pala, K. Thyagarajan, S. Han, D. P. Tsai, and H. A. Atwater, "Gate-Tunable Conducting Oxide Metasurfaces," Nano Lett. **16**(9), 5319–5325 (2016).
22. J. Park, J.-H. Kang, S. J. Kim, X. Liu, and M. L. Brongersma, "Dynamic Reflection Phase and Polarization Control in Metasurfaces," Nano Lett. **17**(1), 407–413 (2017).
23. J. Karst, M. Floess, M. Ubl, C. Dingler, C. Malacrida, T. Steinle, S. Ludwigs, M. Hentschel, and H. Giessen, "Electrically switchable metallic polymer nanoantennas," Science **374**(6567), 612–616 (2021).
24. M. Parry, A. Komar, B. Hopkins, S. Campione, S. Liu, A. E. Miroshnichenko, J. Nogan, M. B. Sinclair, I. Brener, and D. N. Neshev, "Active tuning of high-Q dielectric metasurfaces," Appl. Phys. Lett. **111**(5), 053102 (2017).
25. Z. Zhang, Z. You, and D. Chu, "Fundamentals of phase-only liquid crystal on silicon (LCOS) devices," Light: Sci. Appl. **3**(10), e213 (2014).
26. Z. Zhang, A. M. Jeziorska-Chapman, N. Collings, M. Pivnenko, J. Moore, B. Crossland, D. P. Chu, and B. Milne, "High Quality Assembly of Phase-Only Liquid Crystal on Silicon (LCOS) Devices," J. Display Technol. **7**(3), 120–126 (2011).
27. N. Collings, T. Davey, J. Christmas, D. Chu, and B. Crossland, "The Applications and Technology of Phase-Only Liquid Crystal on Silicon Devices," J. Display Technol. **7**(3), 112–119 (2011).
28. Y. Tong, M. Pivnenko, and D. Chu, "Effects of phase flicker in digitally driven phase-only LCOS devices on holographic reconstructed images," Appl. Opt. **61**(5), B25–B33 (2022).
29. M. Pivnenko, K. Li, and D. Chu, "Sub-millisecond switching of multi-level liquid crystal on silicon spatial light modulators for increased information bandwidth," Opt. Express **29**(16), 24614–24628 (2021).
30. Y. Tong, M. Pivnenko, and D. Chu, "Implementation of 10-Bit Phase Modulation for Phase-Only LCOS Devices Using Deep Learning," Advanced Devices & Instrumentation **2020**, 9515747 (2020).
31. Y. Tong, M. Pivnenko, and D. Chu, "Improvements of phase linearity and phase flicker of phase-only LCoS devices for holographic applications," Appl. Opt. **58**(34), G248–G255 (2019).
32. H. Yang, B. Robertson, P. Wilkinson, and D. Chu, "Small phase pattern 2D beam steering and a single LCOS design of 40 1 × 12 stacked wavelength selective switches," Opt. Express **24**(11), 12240–12253 (2016).
33. T. Lu, M. Pivnenko, B. Robertson, and D. Chu, "Pixel-level fringing-effect model to describe the phase profile and diffraction efficiency of a liquid crystal on silicon device," Appl. Opt. **54**(19), 5903–5910 (2015).
34. X. Chang, M. Pivnenko, P. Shrestha, W. Wu, and D. Chu, "Increasing steering angle of LCoS in a WSS system through integration with a metasurface," Appl. Opt. **62**(10), D17–D22 (2023).

Optics EXPRESS

35. X. Song, L. Huang, C. Tang, J. Li, X. Li, J. Liu, Y. Wang, and T. Zentgraf, "Selective Diffraction with Complex Amplitude Modulation by Dielectric Metasurfaces," Adv Opt Mater **6**(4), 1701181 (2018).
36. G. Yoon, J. Jang, J. Mun, K. T. Nam, and J. Rho, "Metasurface zone plate for light manipulation in vectorial regime," Commun. Phys. **2**(1), 156 (2019).
37. Y. Montelongo, J. O. Tenorio-Pearl, C. Williams, S. Zhang, W. I. Milne, and T. D. Wilkinson, "Plasmonic nanoparticle scattering for color holograms," Proc. Natl. Acad. Sci. U.S.A. **111**(35), 12679–12683 (2014).
38. B. Walther, C. Helgert, C. Rockstuhl, F. Setzpfandt, F. Eilenberger, E.-B. Kley, F. Lederer, A. Tünnermann, and T. Pertsch, "Spatial and Spectral Light Shaping with Metamaterials," Adv. Mater. **24**(47), 6300–6304 (2012).
39. H. Cai, J. A. Dolan, G. S. D. Gordon, T. Chung, and D. López, "Polarization-Insensitive Medium-Switchable Holographic Metasurfaces," ACS Photonics **8**, 2581–2589 (2021).

129.169.174.229 {ts '2023-02-27 09:38:11'}